

Machine learning of the Ising model on a spherical Fibonacci lattice

Zheng Zhou,¹ Chen-Hui Song,² Xu-Yang Hou,^{1,*} and Hao Guo^{1,3,†}

¹*School of Physics, Southeast University, Jiulonghu Campus, Nanjing 211189, China*

²*Tsinghua Shenzhen International Graduate School, Tsinghua University, Shenzhen 518055, China*

³*Hefei National Laboratory, Hefei 230088, China*

We investigate the Ising model confined to a spherical surface, focusing on its implementation using a Fibonacci lattice. The challenge lies in uniformly covering the spherical surface to enable reliable comparisons with planar models. Monte Carlo simulations and graph convolutional networks(GCNs) are employed to analyze spin configurations at varying temperatures and to identify phase transition temperatures. Although the spherical Fibonacci lattice is sufficiently uniform, there are still some irregular sites, which introduce interesting effects. In the ferromagnetic case, sites with fewer neighbors are more likely to undergo spin flips at low temperatures; however, this is not necessarily true at high temperatures, which could explain why the phase transition temperature is higher compared to the planar Ising model. In the antiferromagnetic case, the presence of irregular sites results in the total energy of the system at zero temperature not being the lowest. Phase transition temperatures are estimated using specific heat analysis and GCNs, revealing T_C values for both ferromagnetic and antiferromagnetic cases. The study underscores the significance of the Fibonacci lattice's geometric properties in understanding spin interactions in microgravity environments.

I. INTRODUCTION

The Ising model is perhaps the simplest statistical spin model, yet it exhibits a wealth of physical phenomena and plays a crucial role across multiple fields of physics. For example, site disorder and tunable quantum fluctuations give rise to a rich variety of ground states[1–8]. The two-dimensional Ising model is among the simplest statistical models to demonstrate a phase transition. Experimentally, the Ising model can be realized using cold-atom quantum simulators[9–13]. Recently, the rapid advancement of space-based technology has driven experimental efforts to confine ultracold atoms on surfaces of various shapes in microgravity[14–24]. Among these adjustable shapes, the sphere or spherical bubble trap has garnered significant research interest, with numerous studies dedicated to exploring its geometric effects on cold atomic gases. In this paper, we focus on the Ising model confined to a spherical surface. Given the fundamental nature of the Ising model, its analysis is crucial for understanding the physical characteristics of spherical atomic gases in a microgravity environment.

The first challenge of this problem is to cover the spherical surface as uniformly as possible. Only in this way can we reliably compare the results with those of the planar square lattice. This requirement excludes the traditional latitude-longitude lattice, as the density of sites near the poles is significantly higher than anywhere else. The most suitable candidate is the Fibonacci lattice, which is essentially the most uniform spherical lattice. We have previously applied it to study the spherical XY model [25], yielding intriguing results about how vortex distribution is significantly influenced by spherical topology.

It is important to note that the Fibonacci lattice is not perfectly uniform, which complicates the analytical study of the Ising model on the Fibonacci sphere. However, by utilizing Monte Carlo(MC) simulations and machine learning techniques, we can determine the spin configurations at various temperatures and identify the phase-transition temperature of the spherical Ising model. The second challenge is that the Fibonacci lattice, being an irregular lattice, lacks an image-like structure. Therefore, powerful tools such as convolutional neural networks (CNNs) cannot be applied directly to the Fibonacci lattice. Instead, we use graph convolutional neural networks(GCNs) to handle irregular lattices, a method that we have previously applied to study the XY model on a spherical Fibonacci lattice[25]. GCNs are effective in classifying different spin phases and successfully predicting the phase-transition temperature. Recently, a study focused on the ferromagnetic Ising model on a Fibonacci-triangulated sphere found that the model exhibits a critical temperature slightly lower than that of a planar triangular lattice[26]. In this paper, we will concentrate on the mostly quadrangulated Fibonacci lattice for both ferromagnetic and antiferromagnetic Ising models, where neighbor interactions are determined by a cutoff radius r_c .

The rest of this paper is organized as follows: In SectionII, we construct the spherical Fibonacci lattice points, ensuring that the number of lattice sites with four nearest neighbors is maximized by selecting an appropriate spin-interaction cutoff radius r_c . SectionsIII and IV present simulations of the spherical ferromagnetic and antiferromagnetic Ising models, respectively, using MC algorithms and GCNs. These sections include graphs illustrating spin configurations, energy and specific heat at various temperatures, as well as the phase transition temperatures for both models. Finally, SectionV concludes the paper.

* houxuyangwow@seu.edu.cn

† guohao.ph@seu.edu.cn

II. SPHERICAL ISING MODEL

The Ising model on a 2D lattice is described by the Hamiltonian:

$$H_{\{s_i\}} = -J \sum_{\langle i,j \rangle} s_i s_j - h \sum_i s_i, \quad (1)$$

where s_i represents the spin at site i , J is the interaction strength and h is the external magnetic field. The first summation runs over all pairs of adjacent spins, with each pair being counted only once. In this paper, we will focus on the case with $h = 0$ for convenience. Ising models can be classified according to the sign of J : If $J > 0$, the interaction is called ferromagnetic; if $J < 0$, it is antiferromagnetic. For irregular lattices, the distance between adjacent spins may not be a constant. Therefore, it is crucial to carefully define the "nearest-neighbor sites", which will be discussed in detail later.

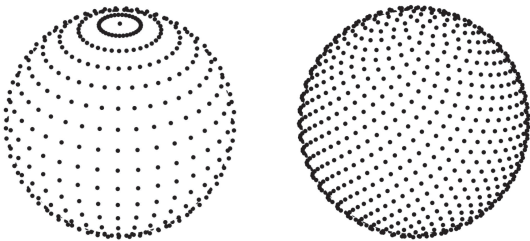


Figure 1. A comparison of the uniformity between two types of lattices of $N = 1000$: the latitude-longitude lattice on the left and the Fibonacci lattice on the right.

The spins of a Fibonacci Ising model are located on a Fibonacci lattice on a spherical surface. The position of each lattice site in Cartesian coordinates is given by:[27–29]

$$\begin{aligned} x_i &= \sqrt{R^2 - z_i^2} \cos(2\pi i \phi), & y_i &= \sqrt{R^2 - z_i^2} \sin(2\pi i \phi), \\ z_i &= R \left(\frac{2i-1}{N} - 1 \right), \end{aligned} \quad (2)$$

where the notation $i = 1, 2, \dots, N$ denotes the index of a lattice point, R represents the radius of the sphere, and $\phi = \frac{\sqrt{5}-1}{2}$ is the golden ratio. Fig.II compares the traditional latitude-longitude lattice with the Fibonacci lattice. Evidently, the latter is considerably more uniform than the former. Next, to compare with the properties of the Ising model on the planar square lattice, we quadrangulate the spherical Fibonacci lattice as much as possible. Equivalent, this means that most spins interact with four nearest neighbors. To achieve this, we set a critical radius r_c . If the distance between two neighboring spins is less than r_c , an interaction is considered to exist between them. To maximize the number of lattice sites with four nearest neighbors in a system with $N = 1000$ lattice sites, we determined the optimal nearest-neighbor radius through exploratory analysis, setting it to $r_c = 0.1298R$.

In this situation, there are 850 spins with 4 neighbors, 76 spins with 3 neighbors, and 74 spins with 5 neighbors. Overall, the 1000 spins have a total of 3998 neighbors, which is very close to the square lattice of $N = 1000$. We connect all "nearest-neighbor sites" and present a two perspectives of the quadrangulation of a $N = 1000$ Fibonacci lattice from two different directions in Fig.II. Most sites appear "regular" except a few having 3 or 5 neighbors. In practical experiments, implementing a Fibonacci lattice is quite straightforward. We simply need to distribute the lattice points as evenly as possible on a spherical surface. This arrangement will naturally approximate a Fibonacci lattice in an appropriate coordinate system, as the Fibonacci lattice is fundamentally the most uniform lattice on a sphere.

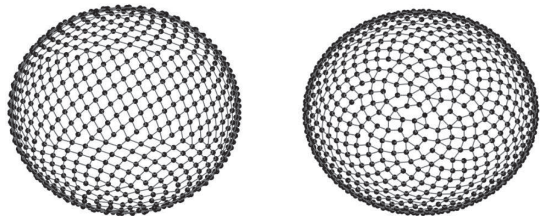


Figure 2. Perspectives of a $N = 1000$ Fibonacci lattice from different directions.

III. FERROMAGNETIC ISING MODEL ON A SPHERICAL FIBONACCI LATTICE

We first consider the case with $J > 0$, in which neighboring sites tend to align with the same spin orientation. This is referred to as the spherical ferromagnetic Ising model. When mapping the Ising model on a spherical Fibonacci lattice, r_c serves as a cutoff range of the interaction. We set $J = 1$, $N = 1000$ and $r_c/R = 0.1298$, and use the MC techniques to obtain samples of spin configurations. We randomly flip the spins in the system and accept or reject state transitions based on the Metropolis criterion. Specifically, if the energy of the system decreases after a flip, the flip is accepted; otherwise, it is accepted only with a certain probability, known as the acceptance probability. As the temperature decreases, the acceptance probability gradually decreases and eventually reaches equilibrium.

At low temperatures, it is evident that all sites have the same spin orientation. As the temperature starts to increase, thermal fluctuations may cause spins at certain sites to reverse direction. However, it is not until the temperature reaches around $T/J \sim 1.9$ that the number of reversed spins becomes fairly considerable. In the top panel of Fig.III, we plot the stable spin configuration at a relatively low temperature of $T/J = 2.0$, where up and down spins are represented by white and black pixels, respectively. It is observed that some spins are flipped (black points), while the majority of the re-

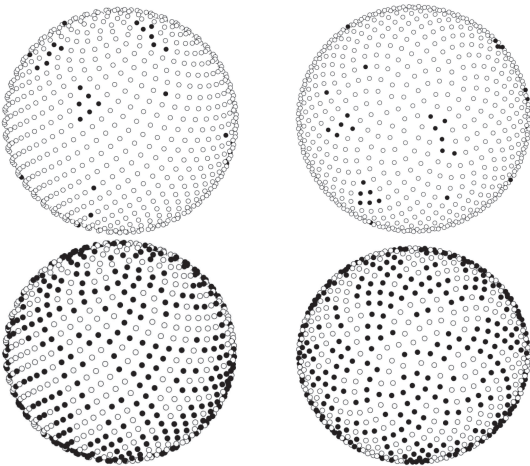


Figure 3. Spin configuration of the spherical ferromagnetic Ising Model at $T/J = 2.0$ (Top panel) and $T/J = 8.0$ (Bottom panel): the left panel shows the front view, while the right panel presents the top view. Up and down spins are white and black pixels.

gions remain predominantly occupied by up spins (white points). Clearly, the system is in the ordered phase. At a very high temperature of $T/J = 8.0$, a significant number of spins are flipped due to thermal fluctuations. As a result, the numbers of up and down spin sites become roughly comparable. The system is now in the disordered phase, and the corresponding spin configuration is shown in the bottom panel of Fig.III.

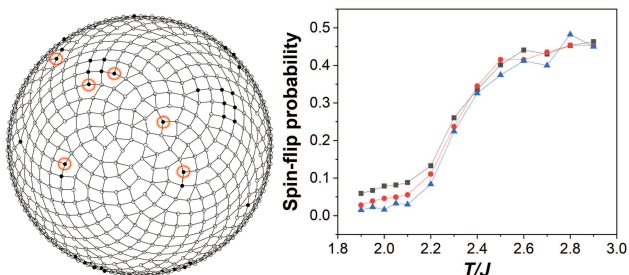


Figure 4. (Left panel) A perspective of the Fibonacci lattice at $T/J = 2.0$, in which the spins at 6 sites with three neighbours change direction. (Right panel) Statistical spin-flip probabilities for spin-flip as a function of temperature.

Note that the Fibonacci lattice is inhomogeneous, with varying probabilities of spin flips at different sites, which is crucial for understanding stable spin patterns. For instance, a site with three neighbors incurs an energy cost of $6J$ to flip its spin, while a site with five neighbors incurs a cost of $10J$. Consequently, the probability of a spin-flip is relatively higher for the site with three neighbors. In Fig.III, we present a view of the Fibonacci lattice from a particular direction at $T/J = 2.0$. It is evident that among the sites where the spin is flipped, at least 6 out of 76 sites have three neighbors. In contrast, only 11 out of 850 sites with four neighbors exhibit spin flips. This

indicates that the proportion of spin flips is relatively significant for sites with three neighbors. We also statistically calculate the average the spin-flip probabilities P_3 , P_4 and P_5 for sites with 3, 4 and 5 neighbours, respectively, across different stable spin configurations at various temperatures. The results are illustrated in Fig.III by black squares representing P_3 , red disks representing P_4 , and blue triangles representing P_5 . Specifically, we perform ten simulations at each temperature. For each simulation, we count the number of spin flips occurring at the sites with 3, 4, and 5 neighbours in a stable spin configuration. We then compute the ratio of these flips to the total number of sites for each type to obtain the flip ratio. Finally, we average the results from the ten simulations at each temperature. At low temperatures, $P_3 > P_4 > P_5$, reflecting that sites with fewer neighbors are more prone to spin flips. At the temperature increases, thermal fluctuations become more significant relative to the energy cost of spin flips, leading to a disruption in the ordering of P_3 , P_4 and P_5 .

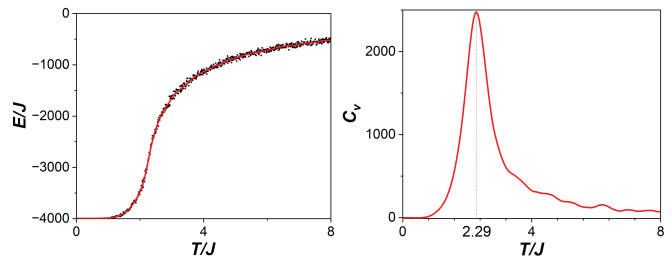


Figure 5. (Left panel) Total energy as a function of temperature for the spherical ferromagnetic Ising model with $N = 1000$. (Right panel) Specific heat as a function of temperature for the same model.

In the end, we aim to determine the phase transition temperature T_c of the spherical Fibonacci Ising model. To achieve this, we employ two different methods. The first method is straightforward but relatively approximate: We estimate T_c by analyzing the behavior of the specific heat C_V . The second method offers greater accuracy and involves using graph convolutional networks (GCN) to refine our estimation of T_c .

Given a stable spin configuration, the total energy E of the system is calculated via Eq.(1). Similarly, we average the total energy over 10 stable spin configuration at each temperature, with a temperature interval $0.01J$. The numerical results are presented in the left panel of Fig.III. To estimate the specific heat, we use the spine functions to fit the E versus T curve, resulting in a function $E(t)$. We then compute the derivative of this function to estimate C_V and plot C_V vs T in the right panel of Fig.III. As shown in the figure, C_V exhibits a singular behavior at $T/J = 2.29$, which can be considered as an estimate of T_c . Interestingly, this value is very close to the critical temperature of the two-dimensional Ising model on a square lattice, which is $T_c^\square/J \simeq 2.269$ [30].

The second approach employs machine learning, which

has proven to be a powerful tool in processing big data[31–38]. Given that the Fibonacci lattice is not homogeneous and does not resemble a typical image-like structure, traditional CNNs can not be applied to this model[39, 40]. Instead, the GCN will be utilized, as it is capable of capturing spatial structural features by leveraging the connectivity relationships between nodes[41]. This makes GCNs particularly well-suited for processing topologically structured data like the Fibonacci lattice. Details of GCN can be found in Appendix A.

We utilize the results from MC simulations as the training samples at both low and very high temperature regimes. The GCN can be subsequently used to identify ordered and disordered phases, as well as phase transitions. To verify the accuracy of the GCN simulations, we investigate two-dimensional square lattices with sizes of 20×20 and 40×40 . The algorithm generates classification confidence values for the ordered phases (p_o) and the disordered phases (p_d), as illustrated in Fig.(III) (with the black solid line representing p_o and the red dashed line representing p_d). As the temperature increases, the black solid line shows a gradual decline from 1, indicating a decreasing similarity between the simulation results and the ordered phase. In contrast, the red dashed line gradually increases from 0, indicating an enhancement in the similarity between the simulation results and the disordered phase. The temperature at which $p_o = p_d$ signifies the phase transition temperature T_c . Through the simulation and analyses of different lattice scales, it is found that as the number of lattice sites increases, the phase transition temperature gradually approaches the theoretical value of $T_c/J \simeq 2.269$. Specifically, the values obtained are $T_c/J = 2.51$ for the 20×20 lattice, and $T_c/J = 2.36$ for the 40×40 lattice. The latter demonstrates a strong concordance with the predicted critical temperature. This indicates that increasing the lattice size can enhance the accuracy of phase transition temperature estimations. Moreover, the GCN effectively captures the phase transition behavior and critical properties.

After validating the accuracy of GCN, we can subsequently use it to calculate the phase transition temperature of the spherical Ising model. In numerical calculation, we select 791 temperature nodes within the range of $[0.1, 8]J$, with an interval of $0.01J$, and perform 100 simulations for each temperature node. The results, shown in Fig.III, indicate that the critical temperature is determined to be $T_c/J = 2.44$. This value is comparatively higher than that obtained from the analysis of the specific heat C_V . Due to the inhomogeneity of the Fibonacci lattice, a complete analytical analysis is not feasible. We believe a possible reason for this discrepancy is the presence of sites with 3 or 5 neighbors, which affects the spin dynamics within the system. At low temperatures, a site with a greater number of neighbors is less likely to experience a spin flip, as verified in Fig.III. However, as the temperature increases, the situation changes. Fig.III shows that $P_4 > P_3 > P_5$ in the range $2.4 \lesssim T/J \lesssim 2.5$,

which indicating that the spins on sites with 3 or 5 neighbors are more difficult to flip. This, to some extent, increases the 'stability' of the ordered phase, which elevating the phase transition temperature.

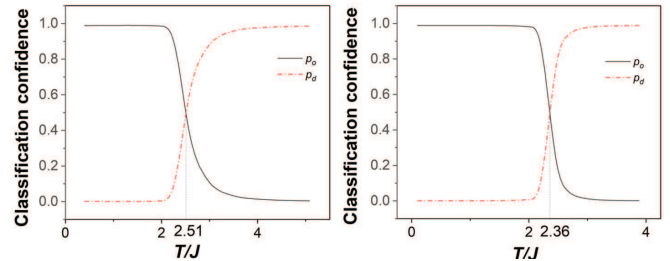


Figure 6. Classification confidences p_o and p_d versus temperature for the 2D Ising model on a 20×20 square lattice(Left panel) and 40×40 square lattice(Right panel).

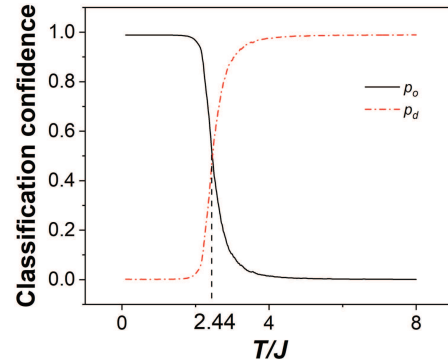


Figure 7. Classification confidences p_o and p_d versus temperature for the ferromagnetic Ising model on a spherical Fibonacci lattice. The phase transition temperature T_c is the point at which $p_o = p_d$.

IV. ANTIFERROMAGNETIC ISING MODEL ON A SPHERICAL FIBONACCI LATTICE

We now consider the case of negative spin coupling, $J < 0$. In this scenario, the nearest spins tend to anti-align, leading to the formation of an ordered antiferromagnetic phase. Consequently, the connectivity features of the lattice will influence the ground-state structures. We set $J = -1$ and focus on the spherical Fibonacci lattice with $N = 1000$ and $r_c/R = 0.1298$. At zero temperature, the MC simulation predicts that most neighboring spins are oppositely aligned. However, the inhomogeneity of the spherical lattice leads to some nearest neighbors exhibiting parallel alignment. The details of the ground-state spin configuration are presented in the left panel of the top row of Fig.IV. As the temperature increases, while remaining low enough, the spin distribution stays in an ordered state, though it becomes irregular at certain sites. We present the corresponding spin configuration

at $T/|J| = 2.0$ as viewed from two different directions in the middle and right panels of the top row of Fig.IV. As the temperature increases sufficiently, the ordered structure is gradually disrupted, resulting in a disordered state similar to that observed in the ferromagnetic Ising model (shown in the bottom row of Fig.III).

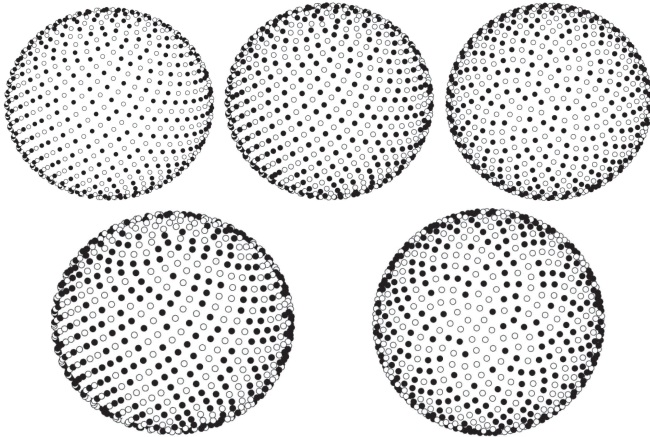


Figure 8. Top row: Spin configurations of the antiferromagnetic Ising model on a spherical Fibonacci lattice at $T/|J| = 0.0$ (left) and at $T/|J| = 2.0$ from two different directions (middle and right). Bottom row: Two perspectives of a stable spin configuration of the same model at $T/|J| = 8.0$.

To determine the phase transition temperature, we will continue using the two previous methods. Following the same procedure, we calculate the total energy for stable spin configurations at each temperature and plot E vs T in Fig.IV. By fitting the $E - T$ curve with spine functions and taking derivatives with respect to T , we obtain the specific heat C_V , which is also presented in Fig.IV. Interestingly, the total energy near zero temperature is not the lowest, which contrasts with the behavior observed in the planar square lattice. This can be explained as follows. The planar square lattice is a bipartite lattice that can be divided into two sub-lattices, with sites from one sub-lattice interacting only with those from the other. If the spins on the two sub-lattices have opposite signs, the total energy is the lowest. When the spins on the two sub-lattices have opposite signs, the total energy is minimized. In the case of the Fibonacci lattice, the sites with 3 or 5 neighbors break this symmetry, leading to an increase in total energy, so that the most uniform spin distribution does not correspond to the lowest energy state. This is, in fact, a distinctive feature of non-uniform lattices. Furthermore, based on the behavior of C_V , we obtain a rough estimation of the critical temperature: $T_c/|J| = 2.09$, which is close to the phase transition temperature of the 2D antiferromagnetic Ising model $T_c^\square/J \simeq 2.269$ [30].

The method based on GCN provides a more accurate estimate to the T_c of antiferromagnetic Ising model on a spherical Fibonacci lattice. We present our numerical results in Fig.IV, where the critical temperature is found

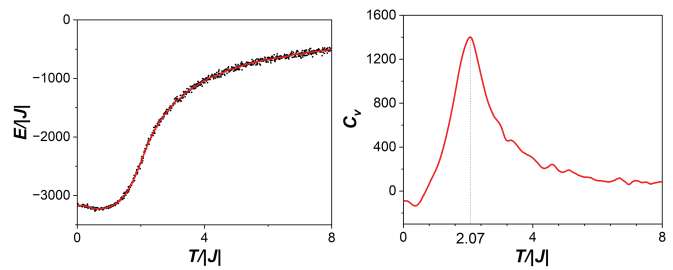


Figure 9. (Left panel) Total energy as a function of temperature for the spherical ferromagnetic Ising model with $N = 1000$. (Right panel) Specific heat as a function of temperature for the same model.

to be $T/|J| = 2.46$. It is fairly close to T_c of the ferromagnetic Ising model on the spherical Fibonacci lattice. This similarity may arise from the resemblance between the spin configurations of the two models at high temperatures: The spin distributions of both are similarly chaotic. Moreover, p_o and p_d exhibit non-smooth behavior in the high-temperature regime. This non-smoothness is due to the inherent ambiguity in the resemblance between spin configurations at low and high temperatures in the spherical antiferromagnetic Ising model, which results in suboptimal performance of the GCN in learning tasks. Nonetheless, despite these challenges, this approach remains instrumental in identifying the phase transition temperature of the model.

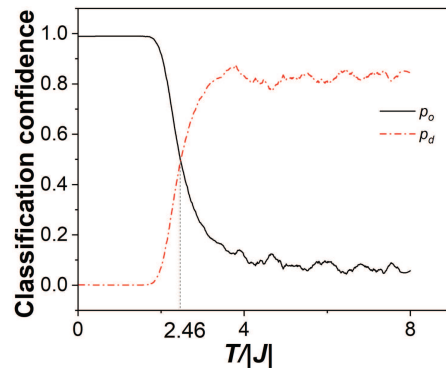


Figure 10. Critical temperature of the antiferromagnetic Ising model on a spherical Fibonacci lattice.

V. CONCLUSION

In this paper, we studied the Ising model on a spherical Fibonacci lattice, employing both Monte Carlo simulations and graph convolutional networks (GCNs) to analyze spin configurations and identify phase transition temperatures. Despite the Fibonacci lattice's relative uniformity, the presence of irregular sites led to significant effects on spin configurations. In the ferromagnetic case, we found that sites with fewer neighbors were more

likely to experience spin flips at low temperatures, while this tendency diminished at higher temperatures, contributing to an increased phase transition temperature compared to the planar Ising model. In the antiferromagnetic case, irregularities in the lattice structure resulted in a scenario where the total energy at zero temperature is not at its minimum, reflecting the complexity of interactions influenced by the lattice geometry.

By utilizing specific heat analysis and GCNs, we successfully estimated the phase transition temperatures for both ferromagnetic and antiferromagnetic cases, revealing values that underscore the impact of geometric properties on spin interactions. Our findings highlight the importance of understanding these geometric features in the context of microgravity environments, paving the way for future research in both theoretical and experimental settings. Overall, this work enhances our comprehension of the Ising model in non-planar geometries and opens avenues for further investigation into the behaviors of spin systems in complex lattice structures.

VI. ACKNOWLEDGMENTS

H.G. was supported by the Innovation Program for Quantum Science and Technology(Grant No.2021ZD0301904) and the National Natural Science Foundation of China(Grant No.12074064). X.-Y. H. was

supported by the Jiangsu Funding Program for Excellent Postdoctoral Talent(Grant No.2023ZB611).

Appendix A: Methodology of phase classification: Details of GCN

In this paper, we use the spherical Fibonacci lattice as a sample, where the lattice information is represented as a graph \mathcal{G} . All relevant data is stored in the degree matrix \mathbf{D} and the adjacency matrix \mathcal{A} . The convolution operation is performed using the Laplacian matrix $\mathbf{L} = \mathbf{D} - \mathcal{A}$.

The features of the lattice points are organized into the feature matrix $\mathbf{X} = (\mathbf{s}_1, \dots, \mathbf{s}_N)^T \in \mathbb{R}^N$, where N is the number of sites and \mathbf{s}_i denotes the spin at lattice site i . We then apply the Random Walk normalized Laplacian $\mathbf{L}^{\text{rm}} = \mathbf{D}^{-1}\mathbf{L}$ for feature extraction, combining it with the feature matrix to obtain:

$$\mathbf{H} = \text{ReLu}(\mathbf{L}^{\text{rm}}\mathbf{X}\mathbf{W}_h + \mathbf{b}_h) \quad (\text{A1})$$

Here, ReLu serves as the activation function, $\mathbf{W}_h \in \mathbb{R}^{1 \times 1}$ is the weight, and $\mathbf{b}_h \in \mathbb{R}^{N \times 1}$ is the bias. Finally, we employ a fully connected layer along with the *softmax* function to aggregate the hidden layer, resulting in an output $\mathbf{H} \in \mathbb{R}^{N \times 1}$ that generates classification confidence for the ordered and disordered phases, denoted as p_o and p_d . The temperature at which $p_o = p_d$ defines the phase transition temperature T_c .

-
- [1] L. Onsager, *Physical Review* **65**, 117 (1944).
 - [2] C. N. Yang, *Physical Review* **85**, 808 (1952).
 - [3] M. E. Fisher, *Physical Review* **176**, 257 (1968).
 - [4] L. P. Kadanoff, *Physics Physique Fizika* **2**, 263 (1966).
 - [5] B. M. McCoy and T. T. Wu, *Physical Review* **176**, 631 (1968).
 - [6] A. B. Harris, *Journal of Physics C: Solid State Physics* **7**, 1671 (1974).
 - [7] Y. Imry and S. keng Ma, *Physical Review Letters* **35**, 1399 (1975).
 - [8] S. Sachdev, *Quantum Phase Transitions* (Cambridge University Press, 2011), 2nd ed.
 - [9] R. J. Elliott, P. Pfeuty, and C. Wood, *Phys. Rev. Lett.* **25**, 443 (1970).
 - [10] P. P. Orth, I. Stanic, and K. Le Hur, *Phys. Rev. A* **77**, 051601 (2008).
 - [11] H. Labuhn, D. Barredo, S. Ravets, S. de Léséleuc, T. Macrì, T. Lahaye, and A. Browaeys, *Nature* **534**, 667–670 (2016).
 - [12] H. Bernien, S. Schwartz, A. Keesling, H. Levine, A. Omran, H. Pichler, S. Choi, A. S. Zibrov, M. Endres, M. Greiner, et al., *NATURE* **551**, 579+ (2017).
 - [13] C. V. Parker, L.-C. Ha, and C. Chin, *NATURE PHYSICS* **9**, 769 (2013), ISSN 1745-2473.
 - [14] N. Lundblad, R. A. Carollo, C. Lannert, M. J. Gold, X. Jiang, D. Paseltiner, N. Sergay, and D. C. Aveline, *npj Microgravity* **5**, 30 (2019).
 - [15] A. Tononi, F. Cinti, and L. Salasnich, *Phys. Rev. Lett.* **125**, 010402 (2020).
 - [16] R. Carollo, D. Aveline, B. Rhyno, S. Vishveshwara, C. Lannert, J. Murphree, E. Elliott, J. Williams, R. Thompson, and N. Lundblad, *Observation of ultracold atomic bubbles in orbital microgravity* (2021), arXiv: 2108.05880.
 - [17] A. Tononi, A. Pelster, and L. Salasnich, *Phys. Rev. Res.* **4**, 013122 (2022).
 - [18] A. Tononi, F. Cinti, and L. Salasnich, *Phys. Rev. Lett.* **125**, 010402 (2020).
 - [19] A. Tononi and L. Salasnich, *Phys. Rev. Lett.* **123**, 160403 (2019).
 - [20] N. Lundblad, R. A. Carollo, C. Lannert, M. J. Gold, X. Jiang, D. Paseltiner, N. Sergay, and D. C. Aveline, *NPJ MICROGRAVITY* **5** (2019).
 - [21] S. J. Bereta, M. A. Caracanhas, and A. L. Fetter, *Phys. Rev. A* **103**, 053306 (2021).
 - [22] T. van Zoest, N. Gaaloul, Y. Singh, H. Ahlers, W. Herr, S. T. Seidel, W. Ertmer, E. Rasel, M. Eckart, E. Kajari, et al., *Science* **328**, 1540 (2010), <https://www.science.org/doi/pdf/10.1126/science.1189164>.
 - [23] D. Becker, M. D. Lachmann, S. T. Seidel, H. Ahlers, A. N. Dinkelaker, J. Grosse, O. Hellmig, H. Muentinga, V. Schkolnik, T. Wendrich, et al., *NATURE* **562**, 391+ (2018), ISSN 0028-0836.
 - [24] R. A. Carollo, D. C. Aveline, B. Rhyno, S. Vishveshwara,

- C. Lannert, J. D. Murphree, E. R. Elliott, J. R. Williams, R. J. Thompson, and N. Lundblad, *NATURE* **606**, 281+ (2022), ISSN 0028-0836.
- [25] C.-H. Song, Q.-C. Gao, X.-Y. Hou, X. Wang, Z. Zhou, Y. He, H. Guo, and C.-C. Chien, *Phys. Rev. Res.* **4**, 023005 (2022).
- [26] A. S. Pochinok, A. V. Molochkov, and M. N. Chernodub, *Ising model on the fibonacci sphere* (2023), arXiv:2301.06849.
- [27] A. Gonzalez, *MATHEMATICAL GEOSCIENCES* **42**, 49 (2010), ISSN 1874-8961.
- [28] J. H. Hannay and J. F. Nye, *Journal of Physics A: Mathematical and General* **37**, 11591 (2004).
- [29] B. Keinert, M. Innmann, M. Saenger, and M. Stamminger, *ACM TRANSACTIONS ON GRAPHICS* **34** (2015), ISSN 0730-0301, aCM SIGGRAPH Asia Conference, Kobe, JAPAN, NOV 02-05, 2015.
- [30] M. Wadati and Y. Akutsu, in *Solitons*, edited by M. Lakshmanan (Springer Berlin Heidelberg, Berlin, Heidelberg, 1988), pp. 282–306, ISBN 978-3-642-73193-8.
- [31] L. Wang, *Phys. Rev. B* **94**, 195105 (2016).
- [32] G. Carleo and M. Troyer, *Science* **355**, 602 (2017).
- [33] J. Carrasquilla and R. G. Melko, *Nat. Phys.* **13**, 431 (2017).
- [34] K. Ch'ng, J. Carrasquilla, R. G. Melko, and E. Khatami, *Phys. Rev. X* **7**, 031038 (2017).
- [35] D. L. Deng, X. Li, and S. DasSarma, *Phys. Rev. X* **7**, 021021 (2017).
- [36] S. J. Wetzel, *Phys. Rev. E* **96**, 022140 (2017).
- [37] P. Zhang, H. Shen, and H. Zhai, *Phys. Rev. Lett.* **120**, 066401 (2018).
- [38] J. Venderley, V. Khemani, and E. A. Kim, *Phys. Rev. Lett.* **120**, 257204 (2018).
- [39] M. J. S. Beach, A. Golubeva, and R. G. Melko, *Phys. Rev. B* **97**, 045207 (2018).
- [40] W. Zhang, J. Liu, and T.-C. Wei, *Phys. Rev. E* **99**, 032142 (2019).
- [41] J. Zhou, G. Cui, S. Hu, Z. Zhang, C. Yang, Z. Liu, L. Wang, C. Li, and M. Sun, *AI Open* **1**, 57 (2020).